FEBS Letters 355 (1994) 290–296

FEBS 14838

Structure of leech derived tryptase inhibitor (LDTI-C) in solution

Peter Mühlhahn[a], Michael Czisch[a], Robert Morenweiser[b], Bianca Habermann[a], Richard A. Engh[a], Christian P. Sommerhoff[b], Ennes A. Auerswald[b], Tad A. Holak[a,*]

[a]*Max-Planck-Institut für Biochemie, D-82152 Martinsried bei München, Germany*
[b]*Abteilung für Klinische Chemie und Klinische Biochemie in der Chirurgischen Klinik und Poliklinik, Klinikum Innenstadt, LMU München, Germany*

Received 8 September 1994; revised version received 24 October 1994

Abstract The three-dimensional solution structure of the leech derived tryptase inhibitor form C (LDTI-C), an inhibitor of 46 amino acids which contains 3 disulfide bridges, has been determined using 2D NMR spectroscopy. The 3D structure was determined on the basis of 262 interresidue interproton distance constraints derived from nuclear Overhauser enhancement measurements and 25 ϕ angles, supplemented by 3 φ and 15 χ_1 angles. The core of LDTI-C is very well defined and consists of a short 3_{10}-helix-loop and a short two-stranded antiparallel β-sheet between residues 13–14 and 20–21. The N-terminus is fixed to the core by two disulfide bridges, while the C-terminus is connected to the β-sheet via the third disulfide bridge. The binding loop in LDTI exhibits lowest energy conformations belonging to the canonical conformation of serine proteinase inhibitors.

Key words: Tertiary structure; Leech derived tryptase inhibitor; Nuclear magnetic resonance; Tryptase; Kazal-type serine proteinase inhibitor

1. Introduction

The actual physiological functions of the human tryptase, a tetrameric trypsin-like serine proteinase from mast cells, remain to be clarified (for a review see [1]). In vitro studies suggest that the enzyme is involved in the catabolism of extracellular matrix proteins [2], in coagulation [3], and in neuropeptide turnover [4]. Furthermore, a pathogenetic role of tryptase in allergic reactions and destruction of cartilage as in asthma [5], rheumatoid arthritis [6], fibrosis [7], artherosclerosis [8], scleroderma [9], anaphylaxis, and mastocytosis [10], has been implicated.

Recently, Sommerhoff et al. [11] isolated, purified, and characterized new small proteins from *Hirudo medicinalis* which inhibit human tryptase. Three forms were described, designated LDTI-A, LDTI-B, and LDTI-C. Form A, the shortest one, is 42 amino acids long and could not be separated from form B, which contains an additional C-terminal Gly. Form C contains 46 amino acids and has a molecular mass of 4738 Da [11,12]. This form is the subject of our 2D NMR structure determination.

An amino acid sequence comparison of LDTI with other protein inhibitors shows ca. 40% homology of LDTI to Kazal-type inhibitors (ovomucoids), such as turkey ovomucoid 3rd domain (OMTKY3), porcine pancreatic trypsin inhibitor (PSTI), and to the both domains of the Kazal-type-like rhodniin [13], with highest similarity to the non-classical Kazal-type inhibitor bdellin B3 [14]. Rhodniin and bdellin B3 differ from the classical Kazal type inhibitors by their shortened NH-terminal sequences and by one or two internal deletions, respectively. The high identity of these primary structures implied similar 3D structures. Three-dimensional structures of several Kazal type inhibitors are known [15], providing a basis for models, for example, of bdellin B3 and rhodniin [13,14]. Common motifs of the experimentally determined and modeled structures are the exposed 'canonical' binding loop [15], the two to three turn α-helix, and a short three-stranded anti-parallel β-sheet. Distinct differences among the structures are found at the N-termini and at segments connecting the helix with the third β-strand.

In this paper, we describe the three-dimensional structure of LDTI-C in solution as determined by 2D NMR.

2. Experimental

A synthetic gene coding for form C of LDTI was designed, cloned and expressed in *Saccharomyces cerevisiae*. The secreted material was isolated after cross-flow filtration and purified by cation exchange chromatography, it is inhibitorily active and about 85% pure [12]. The sample for NMR contained ~3 mM LDTI-C in 50 mM NaH_2PO_4/CD_3COONa buffer (pH 3.5) in 90% H_2O/10%D_2O. In addition, one sample was prepared in 100% D_2O.

NMR measurements were carried out at 500 MHz and 600 MHz on the Bruker AM-500 and AMX-600 spectrometer, respectively. The following 2D ^1H–^1H NMR spectra were recorded in H_2O and D_2O: NOESY [16] with mixing times of 80 and 100 ms, and TOCSY [17,18] with a MLEV-17 mixing sequence [19] of 50 ms duration. The DQF-COSY spectrum in H_2O and in D_2O were also acquired [20]. All spectra were measured at 27°C. For the NOESY spectra in H_2O, the water resonance was suppressed by the use of a semi-selective excitation pulse in which the last 90° pulse in the sequence was replaced by the jump-return sequence with the carrier placed at the position of water [21]. For the TOCSY and DQF-COSY spectra in H_2O, the water resonance was suppressed by presaturation of the water resonance. For most of the spectra, 700 t_1 increments were collected, each with 4K data points, over a spectral width of 6 kHz in both dimensions. $^3J_{HN\alpha}$ coupling constants were measured from DQF-COSY spectra in H_2O. The apparent $^3J_{HN\alpha}$ coupling constants, measured from the splittings of the NH-C^{α}H cross-peaks, were corrected for line width using a method of Kim and Prestegard [22]. For stereospecific assignment, $^3J_{\alpha\beta}$ were extracted from the DQF-COSY in D_2O. Stereospecific assignments of C^{β}H protons and

*Corresponding author. Fax: (49) (89) 8578-3777.
E-mail: holak@vms.biochem.dpg.de

Abbreviations: LDTI, leech derived tryptase inhibitor; LDTI-C, form C of the leech derived tryptase inhibitor; P1, P2, P3 and P1′, P2′, P3′, designate inhibitor residues amino-terminal and carboxy-terminal of the scissile peptide bond, respectively. NMR, nuclear magnetic resonance; NOE, nuclear Overhauser effect; NOESY, two-dimensional NOE spectroscopy; TOCSY (HOHAHA), total correlation spectroscopy (homonuclear Hartmann-Hahn spectroscopy); DQF-COSY, double quantum filtered homonuclear correlated spectroscopy; 2D, two-dimensional; 3D, three-dimensional; D_2O, deuterated water; SA, simulated annealing; r.m.s., root-mean-square.

SSDI 0014-5793(94)01225-3

methyl groups of valines and leucines were obtained using procedures described by Wagner et al. [23] and Hyberts et al. [24]. An amide exchange experiment, consisting of a series of 2D NOESY experiments, was carried out with LDTI-C lyophilized from water buffer and then freshly dissolved in D_2O. Within 24 h, three 2D datasets were recorded.

Structure calculations were carried out essentially according to the basic protocol described previously [25]. NOEs were derived from the 2D NOESY spectra in H_2O and D_2O at mixing times of 80 and 100 ms, respectively. The intensities of the 2D NOE cross peaks were classified as very strong, strong, medium, weak-medium and weak and converted into distance constraints. A complete list of NOE interproton, hydrogen-bonding distance constraints and torsion angle constraints, as well as coordinates of the structures are available from the authors. The distance constraint data were supplemented with 25 ϕ torsion angle constraints derived from the $^3J_{HN\alpha}$ coupling constant data and 3 φ angles (for the *trans*-peptide bond of the X-Pro residues [26]). ϕ constraints ($-120 \pm 40°$) were introduced corresponding to $^3J_{HN\alpha}$ coupling constants larger than 8 Hz [27]. Stereospecific assignments were obtained for 15 of the 86 prochiral centers of LDTI. For the final refinement, the NOE tables were supplemented with the ϕ constraints derived for coupling constants equal to 8 Hz and ≤ 6 Hz [25]. These ϕ constraints were introduced for residues for which ϕ's were close to the mean value (within $\pm 10°$) and fulfilled the Karplus relationship [27] in structures calculated without the dihedral constraints. Two hydrogen bonds identified on the basis of the examination of the structures during the secondary structure analysis were also introduced. In addition, 25 non-NOE constraints were included in the calculations [25].

The distance bounds of the distance constraints were set to $d \pm 0.3$ Å for the distance constraints between 2.3–2.7 Å (very and strong NOEs), to d ± 0.4 Å for the distance constraints between 2.8–3.6 Å (medium NOEs), and to d −0.6 Å/+0.8 Å for distance constraints 3.7–4.5 Å (weak-medium and weak NOEs) [25]. All protons were explicitly defined in the dynamical simulated annealing calculations, in some cases, however, additional terms were added to the upper bounds that correspond to the pseudoatom correction introduced by Wüthrich [26].

Table 1
Chemical shifts (ppm) of LDTI-C at 27°C and pH 3.5

Residue	NH	$C^{\alpha}H$	$C^{\beta}H$	Others
Lys-1	–	4.66	1.75	γ-CH_2 1.18; δ-CH_2 1.31; ε-CH_2 3.01
Lys-2	8.73	4.34	1.76	γ-CH_2 1.38; δ-CH_2 1.72; ε-CH_2 2.86
Val-3	8.41	4.08	1.97	γ-CH_3 1.10, 0.89†
Cys-4	8.64	4.00	3.11, 2.88	
Ala-5	8.72	4.50	1.23	
Cys-6	7.86	5.33	3.06, 2.56†	
Pro-7	–	4.52	2.07, 1.98	γ-CH_2 2.38, 1.78; δ-CH_2 3.92, 3.53
Lys-8	8.72	4.26	1.86	γ-CH_2 1.36; δ-CH_2 1.63; ε-CH_2 2.80
Ile-9	6.88	4.11	1.66	γ-CH_2 1.38, 1.02; γ-CH_3 0.86; δ-CH_2 0.83
Leu-10	8.65	4.64	1.73, 1.22†	γ-CH 1.44; δ-CH_3 0.84
Lys-11	8.87	4.54	1.72†, 1569	γ-CH_2 1.44; δ-CH_2 1.70; ε-CH_2 2.92
Pro-12	–	4.62	1.91, 1.85	γ-CH_2 2.04, 1.50; δ-CH_2 3.63, 3.36
Val-13	8.32	4.73	2.19	γ-CH_3 0.99, 0.57†
Cys-14	8.79	5.25	3.08†, 2.59	
Gly-15	9.77	4.24, 4.76		
Ser-16	9.02	4.02	3.32	
Asp-17	8.46	4.46	2.95†, 2.64	
Gly-18	8.36	3.72, 4.04		
Arg-19	7.74	4.41	1.75, 1.31	γ-CH_2 1.18; δ-CH_2 2.92
Thr-20	8.29	4.99	3.91	γ-CH_3 1.10
Tyr-21	9.20	4.57	2.84†, 2.42	C2,6H 6.91; C3,5H 7.15
Ala-22	8.92	3.87	1.40	
Asn-23	7.15	4.94	3.37, 3.01†	γ-NH_2 6.42/7.95
Ser-24	9.52	3.94	3.36	
Cys-25	8.07	4.21	3.4, 3.07†	
Ile-26	8.25	3.63	1.83	γ-CH_2 0.91, γ-CH_3 1.18
Ala-27	7.37	2.82	0.90	
Arg-28	7.91	3.99	1.89, 1.73	γ-CH_2 1.60; δ-CH_2 3.15
Cys-29	8.56	4.16	3.52, 3.32	
Asn-30	7.46	4.57	2.88, 2.46†	γ-NH_2 7.49/7.37
Gly-31	7.96	3.98, 3,78		
Val-32	7.34	4.27	1.91	γ-NH_3 0.91, 0.64
Ser-33	8.04	4.43	3.82	
Ile-34	8.59	3.92	1.78	γ-CH_2 1.39/0.81; γ-CH_3 0.98; δ-CH_3 0.69
Lys-35	9.24	4.26	1.62, 1.42†	γ-CH_2 1.30; δ-CH_2 140; ε-CH_2 3.12
Ser-36	7.76	4.53	3.86†. 3.81	
Glu-37	8.61	4.33	2.11, 1.9†	γ-CH_2 2.27, 2.36
Gly-38	8.10	4.25, 3.53		
Ser-39	7.82	4.14	3.72	
Cys-40	8.41	4.67	3.08, 2.48	
Pro-41	–	4.45	2.00, 1.91	γ-CH_2 3.74/2.27; δ-CH_2 3.59
Thr-42	8.18	4.25	4.18	γ-CH_3 1.15
Gly-43	8.31	3.91		
Ile-44	7.91	4.09	1.78	γ-CH_2 1.37/1.09; γ-CH_3 0.83; δ-CH_2 0.76
Leu-45	8.29	4.36	1.55	δ-CH_3 0.79/0.86
Asn-46	7.23	3.17		

†The chemical shifts of $H^{\alpha 1}$, $H^{\beta 2}$, or $C^{\gamma 1}H_3$ protons (IUPAC notation).

3. Results and discussion

The NMR spectra of LDTI were assigned with the conventional 2D NMR methods based on the following spectra: NOESY, TOCSY, and COSY [26]. Proton resonances of all backbone and side chain atoms were assigned with the exception of the α proton of residue 43 (Table 1). In general the spectra had few overlaps. The side-chain NH protons of arginines and lysines were not observed in the spectra. An example of the quality of the NOESY spectrum is shown in Fig. 1. There are three proline residues in the sequence, Pro-7, Pro-12 and Pro-41; all of them have *trans*-peptide bond conformations (as inferred from the presence of the $C^{\alpha}H(i)$-$C^{\delta}H(i+1)$ cross-peaks in the NOESY D_2O spectra).

Fig. 2 summarizes the sequential and medium-range NOEs between the NH protons and the NH, $C^{\alpha}H$ and $C^{\beta}H$ protons, observed in the NOESY spectra of LDTI-C. These NOEs are the basis for the determination of the secondary structure of the protein [26]. For LDTI-C, examination of the pattern of the NOEs suggests the presence of a helix-like structure between residue 24 and 29. Strong sequential NH(i)–NH(i+1) cross-peaks, typical for helices, were found in the spectra. Additionally, NH(i)–NH(i+2) or $C^{\alpha}H(i)$–NH(i+3) connectivities were observed. However, the $C^{\alpha}H(i)$–NH(i+4) and the $C^{\alpha}H(i)$-$C^{\beta}H(i+3)$ cross-peaks, which are necessary to characterize this helix as a α-helix, were missing. On the other hand, the $C^{\alpha}H(i)$-NH(i+2) cross-peaks, typical for a 3_{10}-helix, were present. For a regular 3_{10}-helix, however, one should also observe weak $C^{\alpha}H(i)$-$C^{\beta}H(i+3)$ cross-peaks, which as mentioned above are not observed. This segment of the protein can then be best described as a 3_{10}-helix-loop.

LDTI-C contains 6 cysteine residues and thus 3 disulfide bridges are possible. Based on the homology of LDTI-C to ovomucoid 3rd domain and other Kazal inhibitors, we predicted disulfide pairing between Cys-4–Cys-29, Cys-6–Cys-25, and Cys-14–Cys-40. This combination was indeed confirmed by NOE contacts among the $C^{\beta}H$ and $C^{\alpha}H$ protons of corresponding cysteine residues in the disulfide bridges. Since, how-

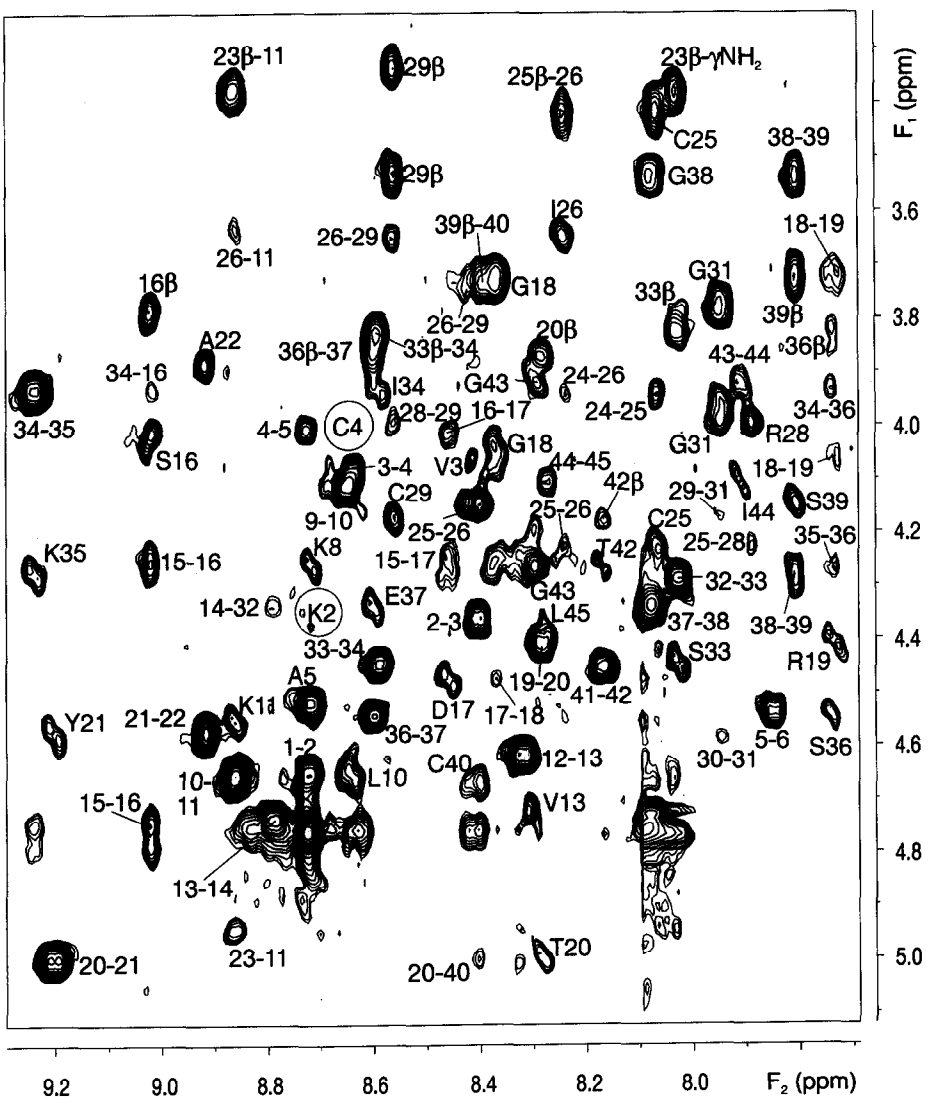

Fig. 1. The NH-$C^{\alpha}H$ region of 2D NOESY spectrum of LDTI-C. Intraresidue cross-peaks are labeled with one-letter abbreviations and interresidue connectivities are indicated by simple numbers. The intraresidue cross-peaks of K2 and C4 are circled at positions corresponding to the TOCSY NH-$C^{\alpha}H$ cross-peaks.

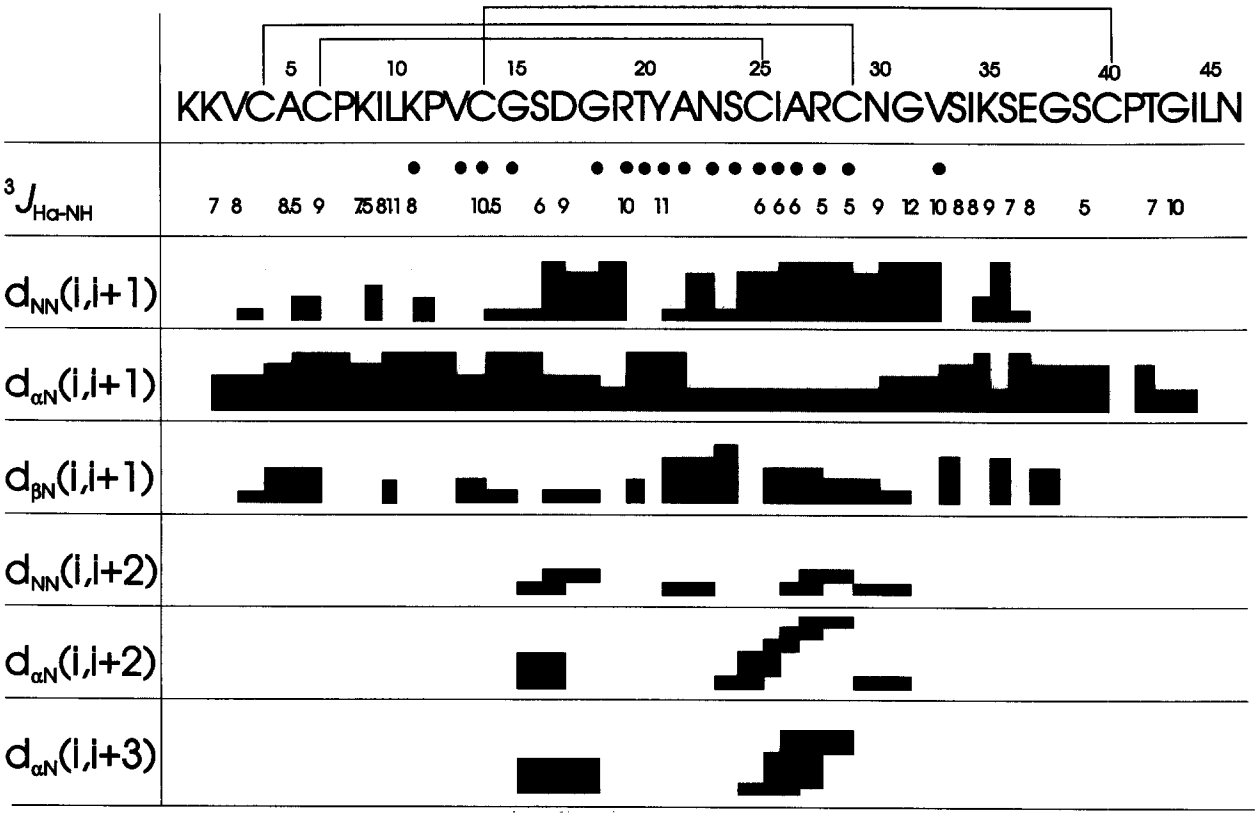

Fig. 2. Amino acid sequence of LDTI-C and survey of NMR data used for identifying secondary structure. The NOEs ($|i-j|<5$), classified as weak, medium, strong, and very strong, are represented by the heights of the bars and were extracted from the NOESY spectra with mixing times of 100 ms. The $C^{\alpha}H(NH)(i)$–$C^{\delta}H(i+1)$ (Pro) NOE is shown along the same line as the $C^{\alpha}H(NH)(i)$–$NH(i+1)$ connectivities. Filled circles indicate NHs that did not exchange against D_2O after 6 h. The values of the $J_{C\alpha H\text{-}NH}$ coupling constants (in Hz) are indicated below the sequence. The disulfide pairing is C4–C29, C6–C25 an C14–C40.

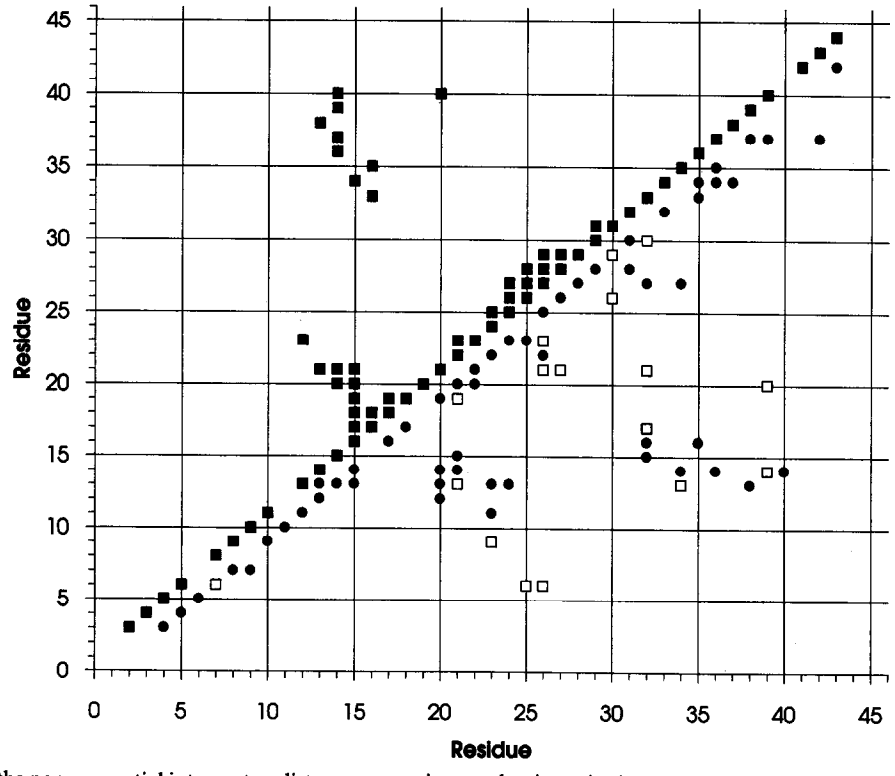

Fig. 3. Diagonal plot of the non-sequential interproton distance constraints used as input in the calculations. Backbone–backbone interactions (filled squares) are plotted above the diagonal; backbone–side chain (circles) and side chain–side chain (squares) constraints are shown below the diagonal.

ever, Cys-4 and Cys-6 are close to each other, the initial structures were calculated without the presence of the disulfide bridges, i.e. no corresponding disulfide distance constraints nor S–S bonds were introduced in the calculations [25]. These structures also indicated the predicted disulfide pairing and in the final calculations the S–S bridges were treated as normal bonds.

The three-dimensional structure of LDTI-C was calculated from 262 approximate interresidue distance constraints (no intraresidue constraints were used). This number of constraints corresponds to the almost complete assignment of all cross-peaks in the NOESY spectra. A total of 20 structures were calculated by a hybrid distance geometry-simulated annealing method [25] with the program XPLOR 3.1 [28]. Fig. 3 shows a diagonal plot of the NOEs identified in the LDTI-C NOESY spectra. It can be seen that due to a large number of NOEs the global folding of the peptide chain in the core is uniquely definied (Figs. 3,4). An average number of interresidue constraints per residue in the core of the protein was 18. All structures satisfy the experimental constraints (r.m.s. for residual NOE and dihedral constraint violations were 0.061 Å and 0.83°, respectively) with small deviations from idealized covalent geometry. The average atomic r.m.s. difference for heavy atoms in the core of LTDI (residues 4–34) among the structures was 0.4 ± 0.1 Å for the backbone atoms and 1.1 ± 0.3 Å for all atoms. The average r.m.s. difference between pairs of the structures [25] in the ϕ, φ angles was < 25° and <40°, respectively. Larger r.m.s. differences were observed for the C- and N-terminus (ca. 3 Å for the backbone atoms).

Fig. 4 indicates that the backbone of LDTI-C is well determined with the exception of residues 1–3 and the C-termini residues from 41–46. These two regions of the protein seem to be completely unstructured. There were no long-range NOEs observed for these regions, and the sequential NOEs were much weaker than NOEs of the residues in the core of the protein. Also, the TOCSY peaks were stronger with noticeable reduction in the linewidths compared to the peaks of residues in well structured regions.

The topology of the global fold of LDTI-C and its secondary

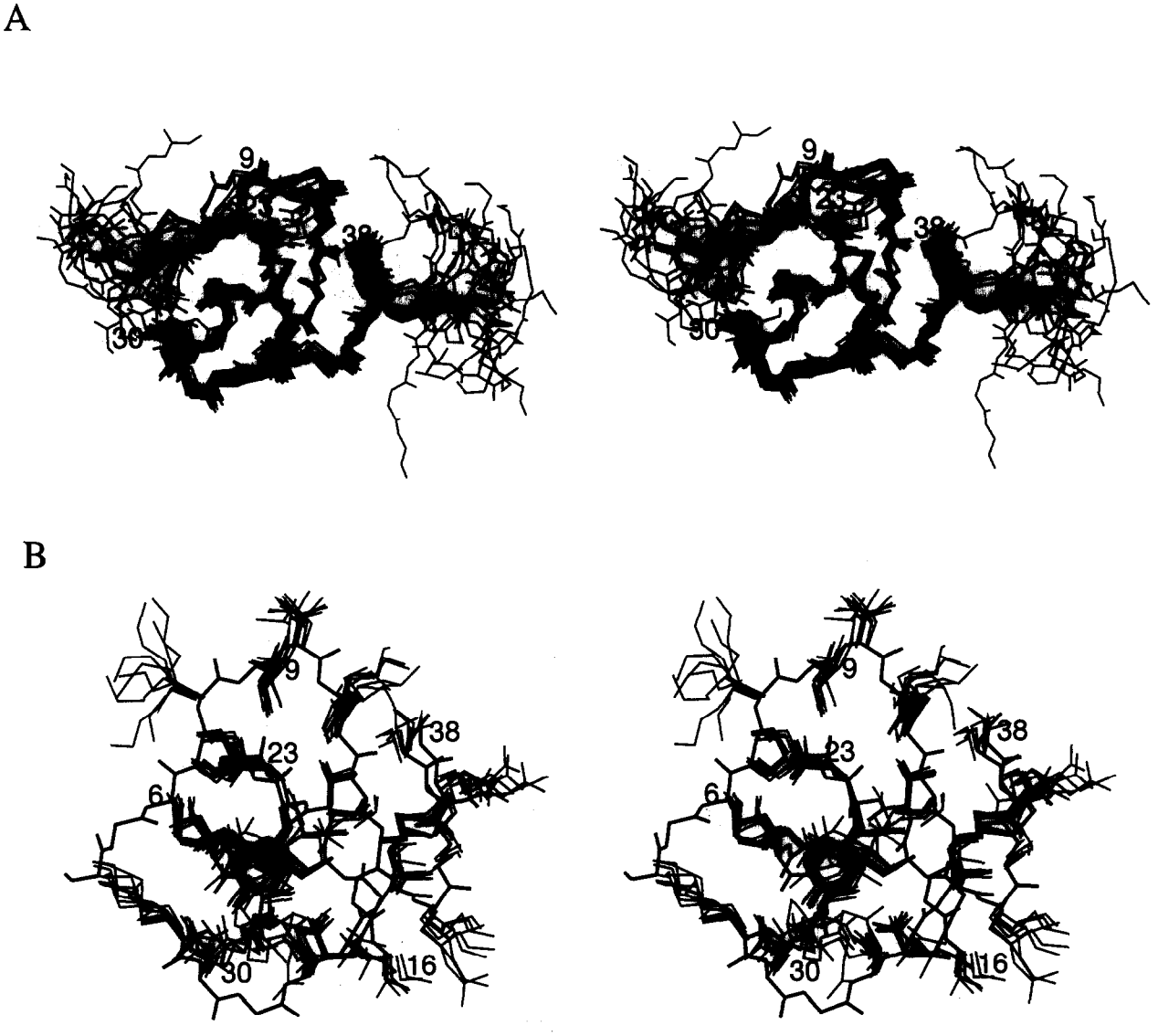

Fig. 4. (A) Stereo view of the backbone atoms (N, Cα, C, and O) of LDTI-C structures best fitted to N, Cα, and C atoms of the residues 12–29. (B) Stereo picture of Cα tracing of LTDI with side chains of residues in the core.

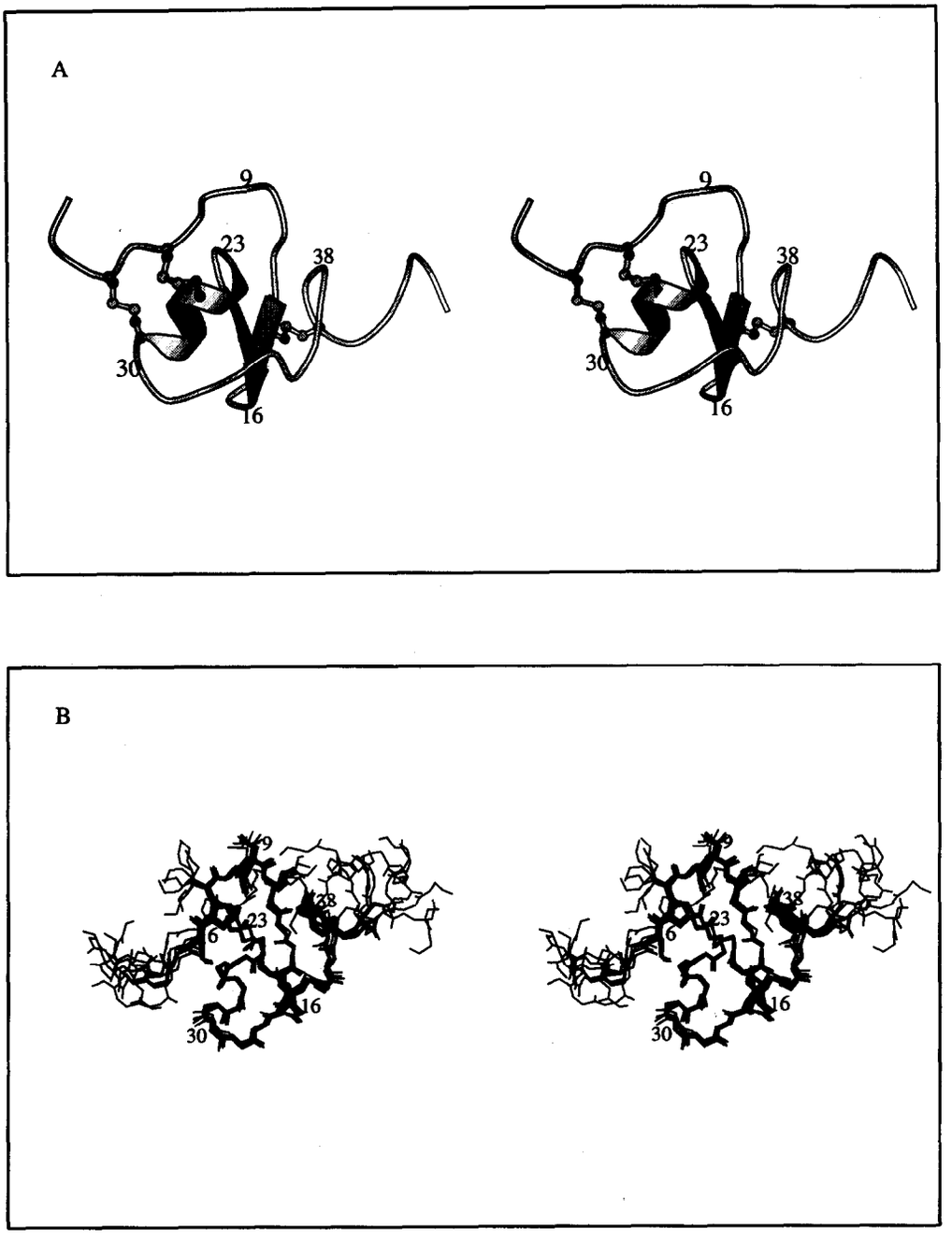

Fig. 5. (A) Ribbon drawing of LDTI-C showing secondary structure and disulfide bridges. (B) Set of the structures that exhibit the canonical conformation of the binding loop (residues 6–12).

structure elements are shown in Fig. 5A. The core of LDTI-C consists of a short one and a half-turn 3_{10}-helix-loop and an extended strand between Asn-30 and Val-32 followed by a loop between Ser-33 and Cys-40. A fragment from Val-13 to Ala-22 may be described as a interstrand connectivity similar to a mini-β-sheet with a reversal at residue 15–19 (Fig. 5A). The strong Cys-14($C^{\alpha}H$)–Thr-20($C^{\alpha}H$) NOE and the medium Val-13(NH)–Tyr-21(NH) NOE is in agreement with such a description.

In general, the conformation of the side-chains are also well defined. Fig. 4B shows that only the side-chain of residues 8, 19 and 28 have greater r.m.s. differences. This may be caused by the inability to make stereospecific assignments for these side-chain protons. A second reason is the lack of side-chain/side-chain contacts (Fig. 3) and long-range NOEs for these residues which makes it impossible to fix the side-chain of these residues.

The N-terminus, which is connected to the helix via two disulfide-bridges, consists of the binding loop between residues 6–12. Residues 4–10 show greater variability compared to the core of LDTI-C in the 20 final structures, which is evident in Fig. 4. This variability is due to the lack of non-sequential

NOEs in this region (as seen in Fig. 3). Only residue Ile-9 has long range contacts to the core of the protein. Thus this region of the strand is connected to the core exclusively via the disulfide-bridges and residue Ile-9. There was, however, a set of structures with a conformation of the binding loop shown in Fig. 5B. Although in no structures were there violations of the NOEs larger than 0.4 Å for loop residues, structures in Fig. 5B best fulfilled all the NOE and (especially) dihedral constraints. This is reminiscent of the situation found in conformations of the binding loop of CMTI-I [29]. In the case of CMTI-I, however, it was possible to choose a unique conformation of the trypsin binding loop from a family of different conformations because only this conformation matched the relative pattern of NOEs. For LDTI-C, other conformations of the binding loop fit the pattern of NOEs in the loop, although most can be eliminated due to unfavorable ϕ-φ angles (ϕ and φ angles were for Pro-7 $-85 \pm 5°$ and $65 \pm 15°$, Lys-8 $-130 \pm 20°$ and $20 \pm 45°$, Ile-9 $-115 \pm 25°$ and $120 \pm 40°$, Leu-10 $-120 \pm 20°$ and $40 \pm 25°$, respectively. For the conformations of Fig. 5B these angles were: Pro-7 $-70 \pm 1°$ and $143 \pm 3°$, Lys-8 $-114 \pm 2°$ and $45 \pm 5°$, Ile-9 $-75 \pm 1°$ and $173 \pm 3°$, Leu-10 $-92 \pm 1°$ and $62 \pm 2°$, respectively).

The best fit conformation of the binding loop corresponds to the 'canonical conformation', a conformation of the residues surrounding the scissile bond (residues P3–P3′) which is highly conserved among serine proteinase inhibitors [15,29] and which enables binding to the target protease. In LDTI-C, the following residues comprise this canonical loop: Cys-6 (P3), Pro-7 (P2), Lys-8 (P1), Ile-9 (P1′), Leu-10 (P2′), and Lys-11 (P3′). Lys-8, at position P1, is the primary determinant of specificity of the inhibitor, consistent with trypsin inhibition, and though disordered, is exposed and poised for insertion into the specificity pocket [15]. A proline residue is found at position P2 also in CMTI [29] and ovomucoid inhibitors [15] and in all cases adopts the canonical conformation.

Prior to this structure determination, analysis of the interactions of LDTI with tryptase relied on modelled structures, which in turn were based on the assumption of the 'canonical conformation' of the binding loop, on the disulfide bridge pattern of Kazal-type inhibitors, and on the modelled structure of bdellin [14]. LDTI and bdellin have a high similarity (55%), and may be aligned without gap insertion, so the model of LDTI differed from bdellin essentially only in the minimized positions of the side chains. Both models are very similar to the NMR structure in their overall fold and are generally confirmed by the NMR structures. The major difference is the flexibility seen at both termini. The termini are near the binding loop, and so may interact in unpredictable ways with tryptase or other target enzymes. Such interactions may contribute to the specificity of binding to tryptase, which, for example, is inhibited by LDTI but not bdellin. Further specificity may arise from interactions with insertions in loops adjacent to the reactive center, whose structures are not known.

Acknowledgments: We thank Robert Huber, Wolfram Bode, Hans Fritz, and Milton Stubbs for stimulating discussions, and Karin Höfling for help in the assignments of the spectra. This work was supported by research grants (H2, H4, H6, G11) from the DFG Sonderforschungbereich 207 of the Ludwig-Maximilians Universität.

References

[1] Eklund, K.K. and Stevens, R.L. (1993) in: Innovations in Proteases and Their Inhibitors (F.X. Aviles ed.) Walter de Gruyter, Berlin, pp. 241–257.
[2] Schwartz, L.B., Metcalfe, D.D., Miller, J.S., Earl, H. and Sullivan, T. (1987) N. Engl. J. Med. 316, 1622–1626.
[3] Maier, M., Spragg, J. and Schwartz, L.B. (1983) J. Immunol. 130, 2532–2536
[4] Caughey, G.H., Leidg, F., Viro, N.F. and Nadel, J.A. (1988) J. Pharmacol. Exp. Ther. 244, 133–137.
[5] Wenzel, S.E., Fowler, A.A. and Schwartz, L.B. (1988) Am. Rev. Respir. Dis. 137, 1002–1008
[6] Stevens, R.L., Somerville, L.L., Sewll, D., Swafford, J.R., Levi-Schaffer, F., Caulfield, J.P., Hubbard, F. and Dayton, E.T. (1992) Arthritis Rheum. 35, 325–335.
[7] Claman, H.N. (1989) J. Am. Med. Assoc. 262, 1206–1209.
[8] Kokkonen, J.O. and Kovanen, P.T. (1989) J. Biol. Chem. 264, 10749–10755
[9] Hawkins, R.A., Claman, H.N., Clark, R.A.F. and Steigerwald, J.C. (1985) Ann. Int. Med. 102, 182–186.
[10] Schwartz, L.B., Bradford, T.R., Littmann, B.L. and Wintroub, B.U. (1985) J. Immunol. 135, 2762–2767.
[11] Sommerhoff, C.P., Söllner, C., Mentele, P., Auerswald, E.A. and Fritz, M. (1994) Biol. Chem. Hoppe-Seyler (submitted).
[12] Auerswald, E.A., Morenwieser, R., Sommerhoff, C.R., Piechottka, G., Eckerskorn, C., Gürtler, C. and Fritz, M. (1994) Biol. Chem. Hoppe-Seyler (submitted).
[13] Friedrich, T., Kröger, B., Bialojan, S., Lemaire, H.G., Höffken, H.W., Reuschenbach, P., Otte, M. and Dodt, J. (1993) J. Biol. Chem. 268, 16216–16222.
[14] Fink, E., Rehm, H., Gippner, C., Bode, W., Eulitz, M., Machleidt, W. and Fritz, H. (1986) Biol. Chem. Hoppe-Seyler 367, 1235–1242.
[15] Bode, W. and Huber, R. (1992) Eur. J. Biochem. 204, 433–451.
[16] Macura, S., Huang, Y., Suter, D. and Ernst, R.R. (1981) J. Magn. Reson. 43, 259–281.
[17] Braunschweiler, L. and Ernst, R.R. (1983) J. Magn. Reson. 53, 521–558.
[18] Davis, D.G. and Bax, A. (1985) J. Am. Chem. Soc. 107, 2821–2822.
[19] Bax, A. and Davis, D.G. (1985) J. Magn. Reson. 65, 355–366.
[20] Ernst, R.R., Bodenhausen G. and Wokaun, A. (1987) Principles of Nuclear Magnetic Resonance in One and Two Dimensions, Clarendon Press, Oxford.
[21] Plateau, P. and Gueron, M. (1982) J. Am. Chem. Soc. 104, 7310–7311.
[22] Kim, Y. and Prestagard, J.H. (1989) J. Magn. Reson. 84, 9–13.
[23] Wagner, G., Braun, W., Havel, T.F., Schaumann, T., Go, N. and Wüthrich, K. (1987) J. Mol. Biol. 196, 611–639.
[24] Hyberts, S.G., Mäki, W. and Wagner, G. (1987) Eur. J. Biochem. 164, 625–635.
[25] Holak, T.A., Gondol, D., Otlewski, J. and Wilusz, T.J. (1989) J. Mol. Biol. 210, 635–648.
[26] Wüthrich, K. (1986) NMR of Proteins and Nucleic Acids, Wiley, New York.
[27] Pardi, A., Billeter, M. and Wüthrich, K. (1984) J. Mol. Biol. 180, 741–751.
[28] Brünger, A.T. and Nilges, M. (1993) Q. Rev. Biophys. 26, 49–125.
[29] Holak, T.A., Bode, W., Huber, R., Otlewski, J. and Wilusz, T.J. (1989) J. Mol. Biol. 210, 649–654.